

Noise decomposition of dual synchronized propellers in hover

Mansi Bhardwaj*, and Tze Pei Chong†
Brunel University London, Uxbridge, UB8 3PH, UK

Paruchuri Chaitanya‡, and Phillip Joseph§
ISVR, University of Southampton, SO17 1BJ Southampton, UK

This experimental study investigates the acoustic characteristics of dual propellers in the side-by-side configuration, and addresses the impact of blade tip-to-tip separation distances and relative blade-to-blade phase angles on the tonal noise generation with a specially designed propeller rig. The parametric study of co-rotating and counter-rotating configurations is performed to emphasize the effect and importance of phase synchronization in producing the tonal components, such as the 1st Blade Pass Frequency (BPF). The linearity of acoustic interference for the side-by-side propellers is investigated through the principle of superimposition. A unique noise decomposition algorithm for various rotation angles is developed to understand the directional behavior of the synchronized propellers. The responses of the 1st BPF noise radiation as a function of the rotation angle under different combinations of rotating direction and blade-to-blade phase angle have been established.

I. Introduction

Urban air mobility (UAM) has emerged as a promising solution to address the increasing congestion in urban areas, offering a new dimension to transportation through electric vertical take-off and landing (eVTOL) aircraft. As these innovative vehicles pave the way for efficient and rapid urban transportation, they face many challenges such as the excess noise generation [1]. Uncomfortable noise pollution caused by the simultaneous use of multiple propellers to propel these vehicles is a major deciding factor limiting their growth [2]. This problem calls for a thorough knowledge of the causes and characteristics of propeller noise in addition to the development of practical mitigation plans that reduce these noise sources.

Single open rotors have been studied heavily for decades to understand their flow and acoustics characteristics [3–7]. Many researches have dedicated to reduce the noise generation by single rotors with minimum expense on its aerodynamics performance. Recent developments in UAM and the basis of their architecture have brought the wave of interests towards multiple propellers that are placed in close proximity against each other. It is recognized that multiple propellers can increase the complexity of noise generation mechanisms. Nevertheless, these noise can be manipulated in many ways. For example, When two rotors are placed side by side, they produce larger level of noise when their separation distance is the smallest. As the the separation distance increases, the radiated noise level by the two propellers will decrease [8]. Although the variation in separation distance does not change the mean thrust of the system, the standard deviation of the thrust fluctuations will be higher when the two propellers are in close proximity [4]. This phenomenon is thought to be caused by the increased turbulent kinetic energy in the space between the two propellers. Similar observations are also made by Lee and Lee [9] in their study of small multi-rotors. They describe the different responses of wake profiles when two rotor are in close proximity, which will result in different levels of unsteady loading that in turn can manipulate the aerodynamic noise radiation. De Vries *et al.* [10], who study three side-by-side rotors in close proximity, also notice that the presence of adjacent propellers deteriorate the performance of the middle propeller. From their CFD study, Zarri *et al.* [11] observe that the helical structure of the vortex is deformed due to the interaction between three co-rotating rotors. They postulate that such deformation would create the unsteady loading on the blade, hence affecting the tonal noise generation. Noise attributes to multi-propeller is also observed to change in characteristics with the direction of rotation of these rotors with respect to each other. For instance, some literature show that the counter-rotation propellers would generate higher noise level than co-rotating propellers [5, 10, 12].

*Doctoral Researcher, Department of Mechanical and Aerospace Engineering, mansi.bhardwaj@brunel.ac.uk, AIAA Student Member.

†Reader, Department of Mechanical and Aerospace Engineering, t.p.chong@brunel.ac.uk, Senior member AIAA.

‡RAEng Research Fellow and lecturer, Institute of Sound and Vibration Research, ccp1m17@soton.ac.uk, and AIAA Member.

§Professor, Institute of Sound and Vibration Research, pfj@soton.ac.uk, Senior member AIAA.

One of the challenges in the design of UAM is the space constraint. In many cases, it might not be feasible to accommodate propellers at considerable separation distance between them. While there are multiple proposed design considerations for the minimal noise generation, most of the options inevitably come at some expense of the propeller performance. Nevertheless, one of the effective method to mitigate noise is to utilize phase synchronization for the propellers. Recent studies have shown that when two identical propellers are rotating with same speed and have same phase angle, the destructive interference can cause a reduction in the noise level at certain directions [5, 13]. Pascioni and Rizzi [14] show that noise can be efficiently reduced by carefully selecting the phases between the two propellers for a more focused directivity. Schiller *et al.* [13] examine the efficiency of rotor phase synchronization in reducing the emitted sound power level. In their findings, phase control technique is considered as a viable technique to reduce tonal noise particularly at the fundamental blade passage frequency (BPF). Vries *et al.* [10], although predominantly interested in the aerodynamic interaction between the propellers for distributed propulsion, conclude that effective synchronization can indeed result in better flow interactions, which in turn lead to reduction in the unsteady loading and the corresponding loading-induced noise. They also conclude that propeller performance is unaffected by the phase synchronization. Similar findings are also reported in [11].

Expanding upon the earlier works, this paper investigates the mitigation of tone at the 1st BPF by the phase synchronization of two side-by-side propellers in both the co-rotating and counter-rotating configurations with various separation distances. The paper discusses a basic analysis to comprehend the directional behaviour of the synchronized propellers for different rotation angles as function of fixed phase difference using a noise decomposition technique. A brief description of this technique along with the experimental setup is given in section II. Section III discusses acoustic results and finally the summary is presented in Section IV.

II. Experimental Setup

The experiments were conducted in an aeroacoustics facility at Brunel University London. The anechoic chamber has a cut-off frequency of approximately 200 Hz. For the acoustic measurements, an array of five G.R.A.S 46AE free-field condenser microphones was employed. Calibration of these microphones was performed using a G.R.A.S 42AB sound calibrator. The noise data in this study is presented in terms of Sound Pressure Level (SPL), band-filtered Overall Sound Pressure Level (OASPL) and band-filtered Overall sound power level (OAPWL). SPL is calculated using the formula as shown below.

$$\text{SPL}(f) = 20 \log_{10} \left[\frac{p(f)}{p_{\text{ref}}} \right], \text{ dB},$$

where f is the frequency in Hz, p_{ref} is the reference pressure equivalent to $20 \mu\text{Pa}$, and $p(f)$ is the root mean square of the measured acoustic pressures. The band-filtered OASPL and OAPWL are determined by integrating the acoustic pressure across ± 20 Hz from the discrete BPF to capture the energy of the tonal peaks.

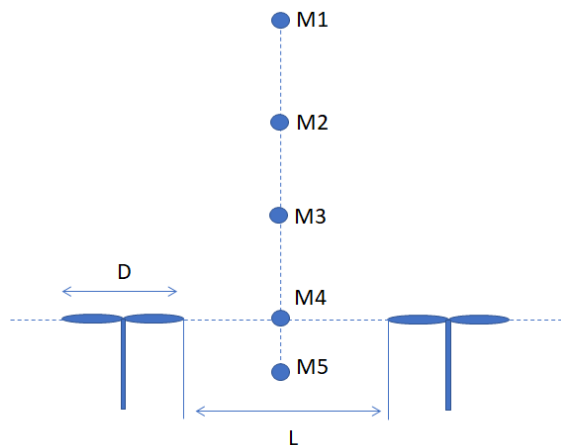


Fig. 1 Schematic of the propeller locations and microphone array (M1-M5). Note that the flow ingestion is from the bottom of the schematic, where the propeller wake will develop upwards.

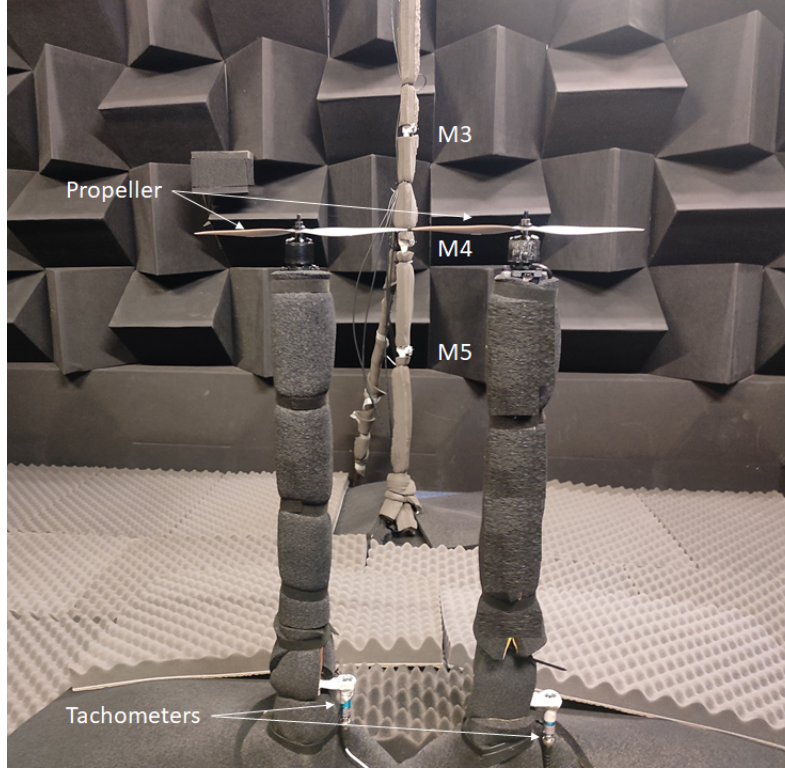


Fig. 2 Photograph of the test setup inside an anechoic chamber.

The experiments utilized two APC 11x4.7 SF propellers mounted at a height of 1 m above the ground in a hover configuration. The microphone array was positioned 1.2 m away from the centre vertical plane between the two propellers as shown in the schematic view in figure 1. Microphone M1 to M3 focuses the propeller wake, M4 aligns with the propeller horizontal plane and M5 is located at the flow ingestion side of the propellers. Note that the flow ingestion is from the bottom and the propeller wake will develop upwards. Figure 2 shows the photographic view of the experimental setup. Two tachometers are used to read the rotational speed of the propellers and act as the triggering devices to identify the rotational phase of individual propellers. The speed of the rotation is maintained by a speed control logic that was set to 5000 rpm.

An analogue-to-digital card from the National Instruments is used to acquire the microphone signal. Data samples were collected for 3 continuous minutes at a sampling rate of 100 kHz, and they were fast Fourier transformed with a window size of 2^{12} points with a partial overlap to produce the acoustical power spectral density. The extensive data sampling time of 3 minutes is necessary to ensure an adequate number of ensembles for the synchronized portions of the data range after discarding all the non-synchronized and uncorrelated data. Such data filtering was performed by delegating the signals from the two tachometers as the triggering sources, which then allow us to pinpoint the phase angle of each propeller and determine the phase angle difference for both propellers. Here, 9 different blade tip-to-tip separation distances, L , were investigated. In the analysis below, each L is normalized by the rotor blade diameter, D . Table 1 summarizes the selection of L/D and their notations.

Notation	d1	d2	d3	d4	d5	d6	d7	d8	d9
L/D	0.02	0.03	0.05	0.07	0.10	0.25	0.50	0.75	1.00

Table 1 Representation of the notation for the normalized tip-to-tip separation distance between propellers, L/D .

III. Results and Discussion

A. Baseline cases (single propeller, or non-synchronized dual propellers)

As shown in Figure 3, the Sound Power Level (PWL) produced by the single propeller is predominantly higher than the unloaded motor noise and ambient noise, except at frequencies around 1 kHz where some contamination by the motor noise might happen. Nevertheless, this does not affect our investigation on the tonal noise corresponding to the 1st BPF. As shown in the figure, the primary BPF is underpinned by a tonal peak occurs at $f_1 = 170$ Hz, which is at least 50 dB above the motor noise. Subsequent peaks in the spectrum correspond to the harmonics of the primary BPF, which occur at nf_1 , where n is an integer. Additionally, there are discernible minor tones occurring at $\frac{1}{2}nf_1$, which are potentially caused by a slight imbalances in blade or motor vibrations.

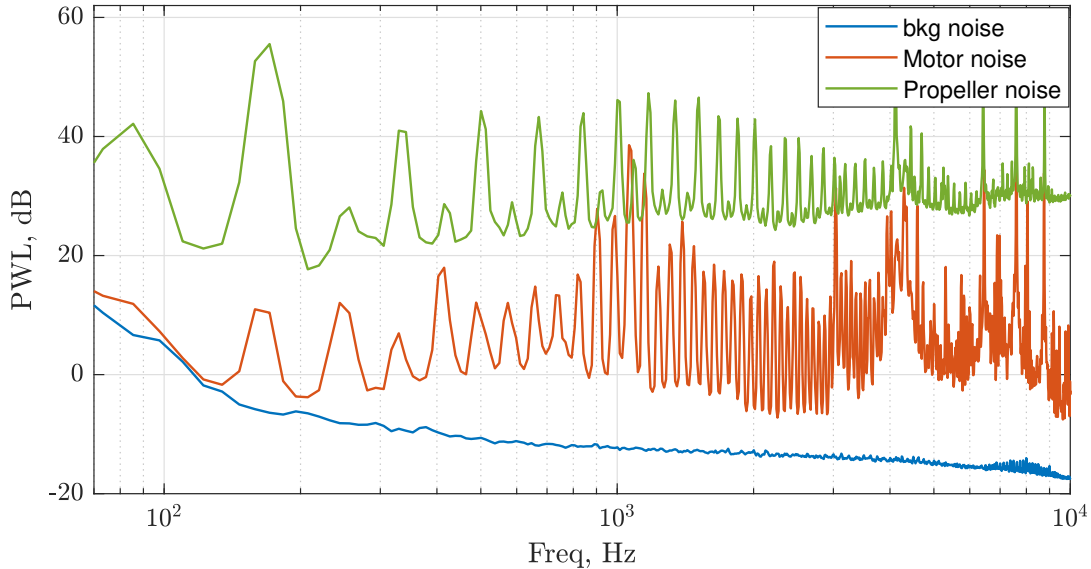


Fig. 3 PWL spectra produced by the single propeller noise, motor noise and background noise.

Acoustic spectra for the non-synchronized dual propellers, both in the co-rotating and counter-rotating configurations, are compared against the acoustic spectrum for a single propeller in Figure 4. The separation tip-to-tip distance between the non-synchronized dual propellers is 0.4 cm, which is the closest distance corresponding to $d1$ in table 1. The presence of additional propeller increases both the tonal and broadband noise components compared to the single propeller case. These phenomena are logical and agree with the literature [8, 15]. For the dual co-rotating and counter-rotating propellers, the tonal noises at the 1st BPF are quite identical in both the radiated sound power level and frequency, which also occurs at $f_1 = 170$ Hz. This indicates that, as far as the tonal noise at the primary BPF is concerned, it is independent of the direction of rotation for the two propellers at $d1$. However, the tonal noise levels for the harmonics at $f = nf_1$ can be sensitive to the direction of rotation between the two propellers, with the counter-rotating one producing the lowest level of harmonic peaks.

Directional patterns of the three cases are shown in figure 5 for the band-filtered Overall Sound Pressure Level (OASPL) for the 1st BPF at $f = 170$ Hz. The polar angles correspond to the microphones M1–M5 cover between -15° and 45° . Note that polar angle of 0° corresponds to the microphone M4, which is in the propeller plane of rotation. Polar angle of -15° represents the flow ingestion plane (M5), where polar angles between 15° and 45° are in the propeller wake (M1–M3). While the single propeller does not exhibit significant directional behavior in the radiated tonal noise for the 1st BPF, the dual propellers would follow a rather peculiar directional pattern. At higher observation angles (between 30° and 45°), as well as the ingestion plane of the propeller (-15°), the radiated band-filtered OASPL by the non-synchronized dual propeller are higher than that produced by the single propeller. However, at polar angle of (15°), a reverse phenomenon occurs. This implies that the near field flow interaction at the propeller tips can cause a destructive interference mechanism on the unsteady loading, which could explain the lower level of tonal noise radiation at the 1st BPF.

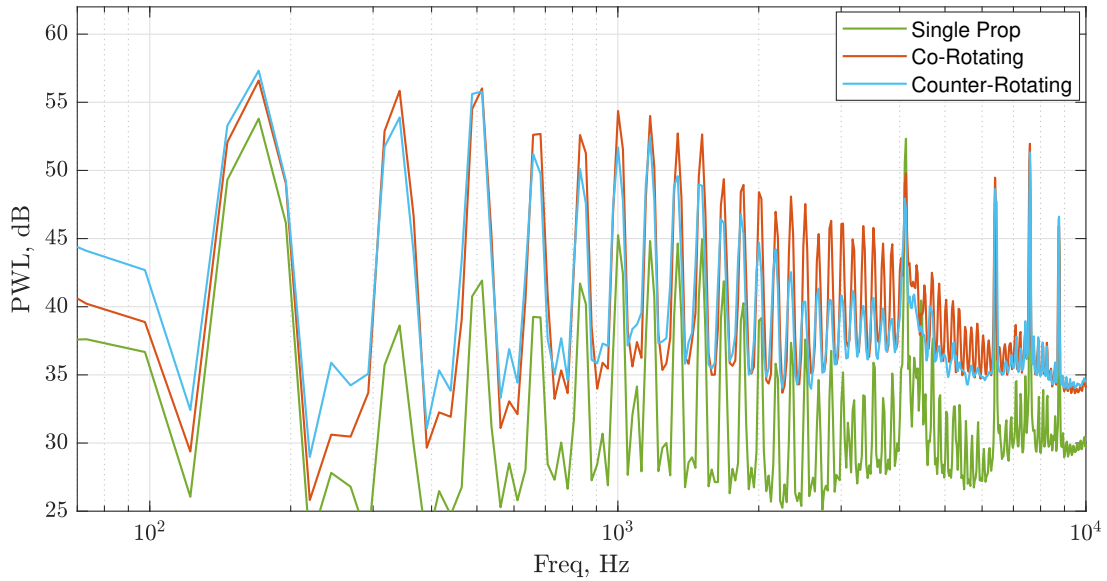


Fig. 4 PWL spectra produced by the single propeller, as well as the non-synchronized dual propellers at the co-rotating and counter-rotating configurations where the tip-to-tip separation distance = $d1$.

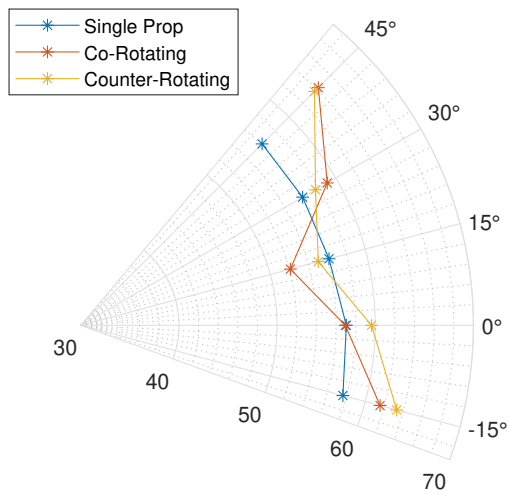


Fig. 5 Comparison of directivity pattern for the band-filtered OASPL, 1st BPF of the single propeller, as well as the non-synchronized dual propellers with both the co-rotating and counter-rotating configurations where the tip-to-tip separation distance = $d1$.

B. Phase-synchronized dual propellers

In this subsection, analysis is performed on the phase-synchronized dual propellers where the aforementioned data-filtering technique is applied to the acquired acoustic data. Here, two geometrical parameters need to be defined first. As shown in figure 6, the orientation of the propeller with respect to the rotational plane can be defined by the ϕ , or 'phi' angle. On the other hand, the angle between the blades for the two propellers is defined as the phase angle between the propellers, θ , or 'theta' angle.

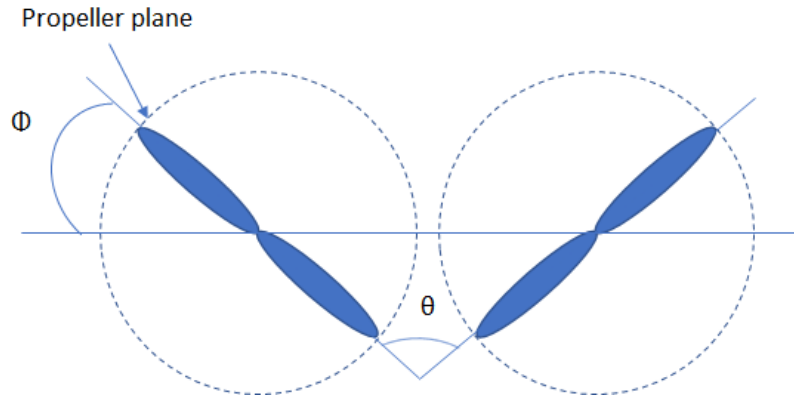


Fig. 6 Sketch illustrating the orientation of the propeller in a rotational plane, (ϕ) or 'phi' angle. The phase difference between two propellers is defined by the θ , or 'theta' angle.

1. Effects of separation distance between the propellers

Different tip-to-tip distances between the two propellers were explored for the optimum noise reduction at the 1st BPF ranging from $d_1 = 4$ mm ($L/D = 0.02$) to $d_9 = 279$ mm ($L/D = 1.0$). Figure 7 shows the band-filtered overall sound power level (OAPWL) for the tonal noise at the 1st BPF as a function of separation distances L/D .

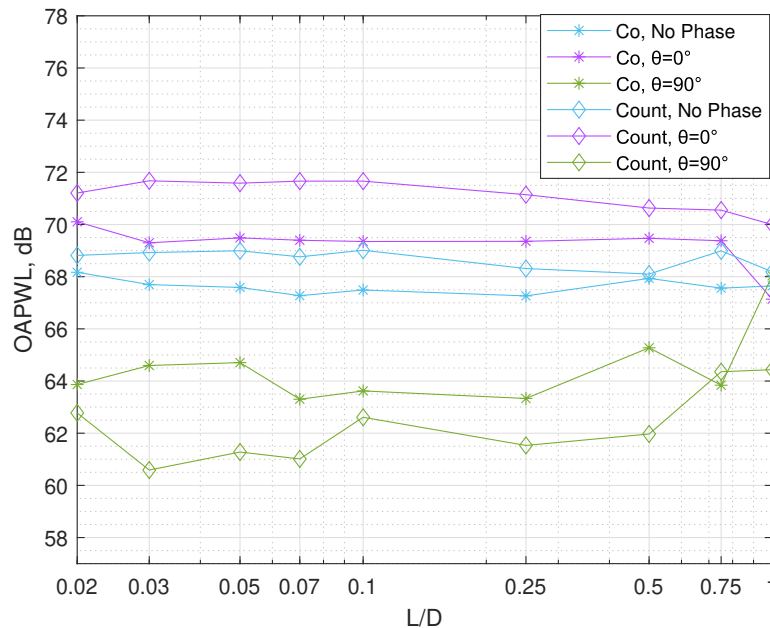


Fig. 7 Band-filtered overall Sound power level at the 1st BPF for the non-synchronised dual propellers (No phase), as well as the synchronised dual propellers whose phase angles θ locked at 0° and 90° , against the tip-to-tip separation distance L/D . The results contain the co-rotating and counter-rotating configurations.

The figure contains two main categories. The first category is the non-synchronised dual propeller, which is abbreviated as (No Phase). Within this category, there is the co-rotating and counter-rotating configurations, abbreviated as 'Co, No Phase' and 'Count, No Phase', respectively. The second category is the synchronised dual propellers, which also contains the division of co- and counter-rotating configurations. Further sub-division can be made by introducing the phase angle, θ . For example, a synchronised dual propeller with counter-rotating configuration where the phase angle $\theta = 90^\circ$ is abbreviated as 'Count, $\theta = 90^\circ$ '.

The analysis begins with the comparison between 'Co, No Phase' and 'Count, No Phase'. While both show little variations of the band-filtered OAPWL as a function of L/D, the former configuration consistently produce about 2 dB lower tonal noise level across the range of L/D except at L/D = 0.5, where the noise is similar to the other configuration. The same trend is qualitatively replicated in the 'Co, $\theta = 0^\circ$ ' and 'Count, $\theta = 0^\circ$ ' cases for the synchronised dual propellers, but the overall level is generally higher than the non-synchronised dual propellers. Interestingly, the low-noise potential of the synchronised dual propellers is manifested when the phase angle (θ) has become 90° for both the co- and counter-rotating configurations. Unlike the previous case, 'Count, $\theta = 90^\circ$ ' shows to be the quietest configuration against all L/D except at L/D = 0.75, at this location, the noise level at 1st BPF is similar to 'Co, $\theta = 90^\circ$ '.

Another interesting observation at in this plot is, at location d9, when the tip to tip distance between the two propellers is equal to the diameter of the propeller (d9), 'Co, $\theta = 0^\circ$ ' and 'Co, $\theta = 90^\circ$ ' converge towards 'Co, No Phase', which is hypothesised to be due to the absence of aerodynamic interaction.

2. Propeller-Propeller interaction

When two or more propellers are in close proximity, the increase in noise can be due to the aeroacoustics interference, or the flow interaction, or the combination of both. The flow interaction becomes weaker with increasing L/D. A preliminary investigation into the interaction noise for the current setup is conducted using the principle of superimposition [16]. This method involves comparing the noise produced by dual propellers when they interact with each other against the sum of noise level generated by individual propellers in isolation.

For this study two extreme tip-to-tip separation distances (d1 and d9) were chosen and the comparison was made for the synchronised co-rotating and counter-rotating dual propellers phase-locked at $\theta = 0^\circ$ and $\theta = 90^\circ$, respectively. Figure 8 shows the PWL spectra for the mentioned combinations. The figure contains (1) the 'Superimposed' spectra, where the acoustic pressure of one single propeller is added with the acoustic pressure of the other single propeller to create the effect of dual propeller without any flow interactions, (2) Dual propeller with $\theta = 0^\circ$, and (3) Dual propeller with $\theta = 90^\circ$

Some intriguing observations emerge from this analysis: At tip-to-tip separation distance of d1, in both the co- and counter-rotating configurations, $\theta = 0^\circ$ exhibits the highest noise level due to significant near field unsteady flow interactions. At $\theta = 90^\circ$, both blade tips will consistently avoid each other. As a result of weaker unsteady flow interaction, the tonal noise level is the lowest. This strongly suggests that at $\theta = 90^\circ$ not only the unsteady flow avoid interacting with each other, but also they might exert some global cancellation effects to reduce the tonal noise level further. Now considering the d9 tip-to-tip separation distance, the co-rotating propellers demonstrate noise levels comparable to the 'Superimposed' spectra. However, for the counter-rotation case, there remains some non-linear interaction.

This comparison study shows that, when tip to tip distance between the two co-rotating propellers reach a distance equal to the diameter of the propeller (d9), noise produced by co-rotating propellers is purely due to acoustic interaction, whereas counter-rotating propellers still show reduced amount of aerodynamic interaction compared to location d1.

3. Decomposition of noise

Results from the previous sections demonstrate the variability of the 1st BPF tonal noise radiation when the synchronised dual propeller is examined under the contexts of different rotating direction (i.e. co- or counter-rotation), and different phase angle between the propellers (i.e. the θ). Noise decomposition of the synchronised single propeller, or synchronised dual propellers under different orientations pertaining to the ϕ as depicted in figure 6 will be discussed in this section. Figure 9 shows the decomposed noise of single propeller at $\phi = 0^\circ, 45^\circ, 90^\circ, 135^\circ$ and 180° pertaining to the band-filtered OASPL measured by microphone M4. As expected, the single propeller generates similar band-filtered OASPL regardless of the ϕ value, which is manifested in figure 9.

Noise decomposition of the tonal peak at the 1st BPF for the synchronised, co-rotating and counter-rotation dual propellers is shown in figure 10 for $\theta = 0^\circ$ and $\theta = 90^\circ$ phase differences. All the results in the figure correspond to the closest tip-to-tip separation distance d1 (L/D = 0.02). Some interesting phenomena have been observed: (1) for all the

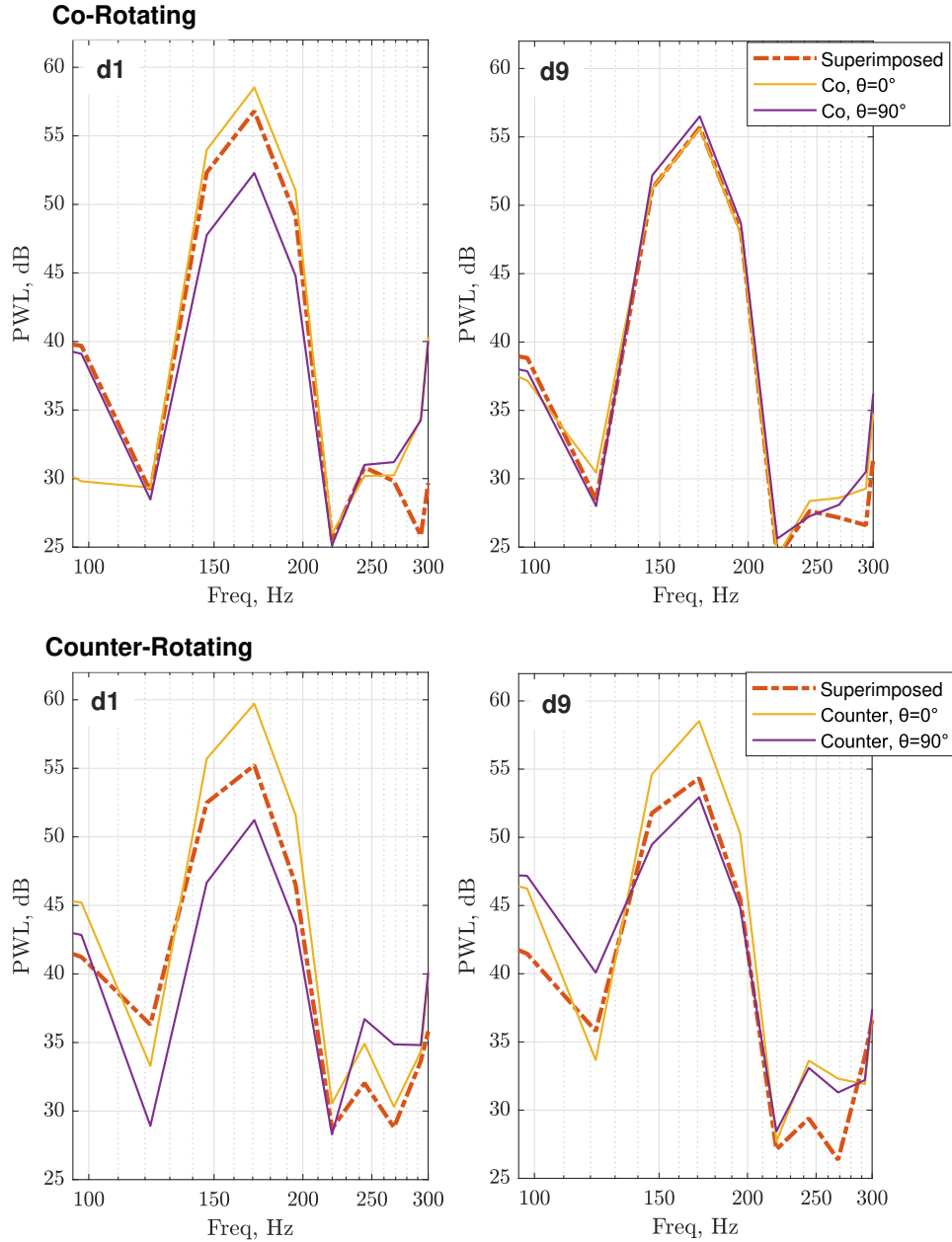


Fig. 8 Comparison of the PWL spectra corresponding to the 1st BPF for single propeller, sum of noise generated by individual propellers in isolation, and dual propellers with different phase angle θ . The configurations of co-rotating and counter-rotating are included. The measurements are performed at two tip-to-tip separation distances: d1 and d9.

configurations, propeller blades at $\phi = 0^\circ$ and $\phi = 180^\circ$ will generate almost the same level of band-filtered OASPL against each other; (2) both the co-rotating and counter-rotating propellers with $\theta = 0^\circ$ will exhibit a 'concave meniscus' shape for the band-filtered OASPL against the ϕ . Conversely, both the co-rotating and counter-rotating propellers with $\theta = 90^\circ$ will exhibit a 'convex meniscus' shape for the band-filtered OASPL against the ϕ ; (3) when the two propellers are in phase, i.e. $\theta = 0^\circ$, the lowest tonal noise radiation happens at $\phi = 90^\circ$. On the other hand, when the two propellers are out of phase, i.e. $\theta = 90^\circ$, the lowest tonal noise radiation happens at $\phi = 0^\circ$ and $\phi = 180^\circ$. With regard to the characteristics described above, similar trends can be observed for the rest of the separation distances d2 to d8. However, at d9 the pattern starts to deviate which could indicate the reduced effect on the propeller-propeller interaction.

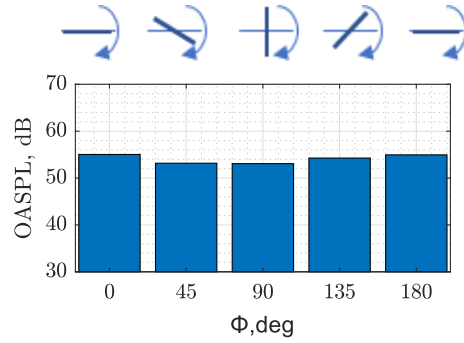


Fig. 9 Band-filtered Overall Sound Pressure level measured at M4 for the 1st BPF as a function of ϕ , angle for the single propeller.

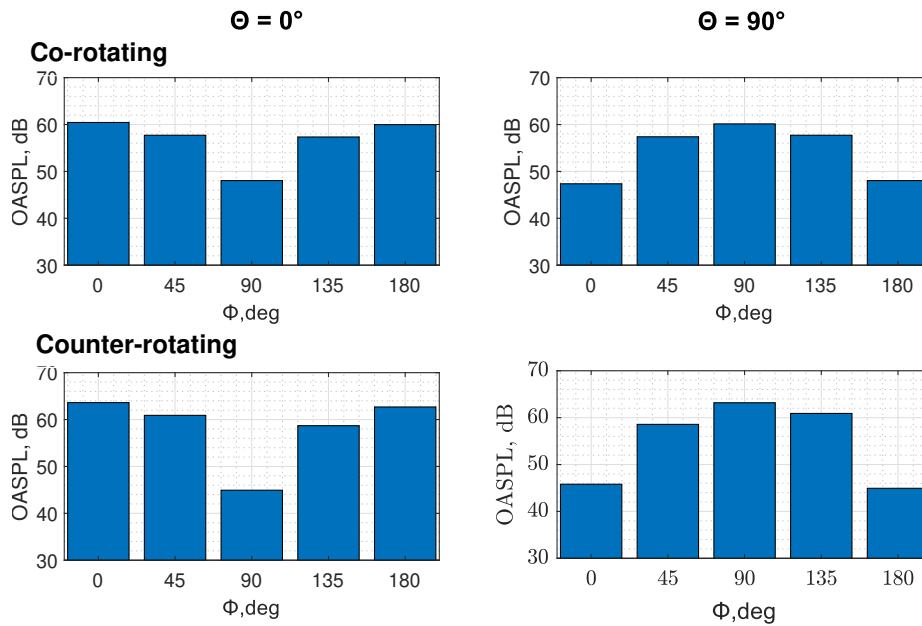


Fig. 10 Band-filtered Overall Sound Pressure Level (Microphone M4) for the 1st BPF as a function of ϕ and θ for co-rotating and counter-rotating propellers. The measurement is performed at the tip-to-tip separation distance = d_1 .

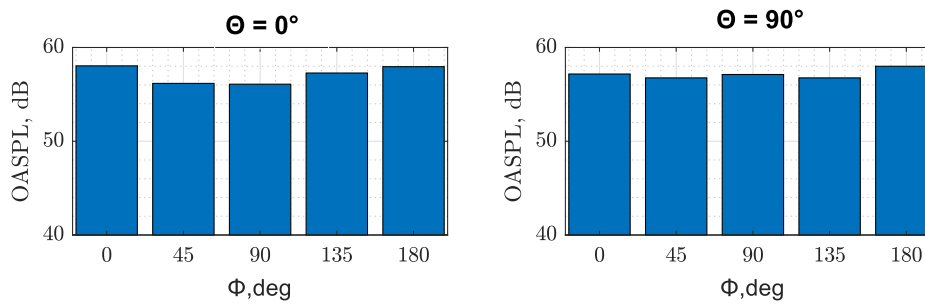


Fig. 11 OASPL against ϕ of the superimposed single propellers to create effects of dual configuration.

Superposition principle, as discussed in III.B.2, was also used with noise decomposition of single propeller to mimic the pattern of the dual co-rotating propellers. Decomposed noise at various azimuthal angles ϕ for a single propeller has been discussed above. Figure 11 shows the decomposed noise pattern for two single propellers added together using superposition principle to make it comparable to dual co-rotating configuration. To imitate co-rotating configuration, acoustic pressure of the two single propellers rotating in same direction was considered. As for 0° phase difference, acoustic pressures for the same ϕ were added together and for 90° phase, a 90° difference was maintained between the two ϕ angles.

On comparing figure 11 with 1st row of figure 10, one can clearly tell the difference. In figure 11, where only acoustic interference is present, both the cases exhibit a consistent pattern amongst themselves, resembling that of a single propeller with only a slight increase in noise levels. Whereas in figure 10, having both acoustic and aerodynamic interference, the decomposition pattern changes for 0° and 90° . This suggests that two propellers, regardless of their rotation direction, when generating noise without any aerodynamic interaction, may behave in a similar way to a single propeller but with a higher level of noise emission.

IV. Conclusion

The study focuses on the analysis of noise characteristics of two propeller in side-by-side configurations. Influencing parameters such as the tip-to-tip separation distances between the propeller, co-rotating and counter-rotating configurations, effect of the propeller phase synchronization at various azimuth/rotation angle, and propeller-propeller interaction are investigated. A special data analysis technique has been developed to decompose the directional elements of the generated noise at the 1st blade pass frequency. The concluding remarks on these studies are as follows:

At $\theta = 0^\circ$ phase angle for the co-rotating and counter rotating dual propellers, the tonal noise at the 1st blade pass frequency will be the loudest compared to the non-synchronized cases. On the other hand, the quieter configuration refer to the $\theta = 90^\circ$ phase angle for the co-rotating and counter rotating dual propellers. Also, between the co-rotating and counter-rotating configurations, the counter-rotating one tends to be quietest for all separation distances. The superposition principle determines the strength of the unsteady flow interaction and how they might affect the tonal noise radiation that relates to the unsteady blade loading. At the closest tip-to-tip separation distance, where the flow interaction between the propellers tends to be strong, the synchronized dual propellers with $\theta = 0^\circ$ generates higher noise level compared to the superimposed level, whereas $\theta = 90^\circ$ generates lesser noise compared to the superimposed spectrum. The orientations of the dual propellers at various rotation angles (ϕ) reveal significant differences in the radiated tonal noise levels. This important observation sheds light on the directional behaviour of the synchronised propellers for $\theta = 0^\circ$ and $\theta = 90^\circ$ phases difference. Irrespective of the direction of rotation of the two propellers, the dual propellers with $\theta = 0^\circ$ will exhibit a 'concave meniscus' shape for the tonal noise level against the ϕ . Conversely, the dual propellers with $\theta = 90^\circ$ will exhibit a 'convex meniscus' shape for the tonal noise level against the ϕ . In the presence of only acoustic interaction, the directional behaviour of the propellers show similar pattern as that of the single propeller for all ϕ .

Although the results presented in this paper suggest a strong interference effect between the propellers, we are motivated to conduct further work to understand the underlying physical mechanisms for a broader array of configurations.

References

- [1] Greenwood, E., Brentner, K. S., Rau, R. F., and Ted Gan, Z. F., "Challenges and opportunities for low noise electric aircraft," *International Journal of Aeroacoustics*, Vol. 21, No. 5-7, 2022, pp. 315–381.
- [2] Rizzi, S. A., Huff, D. L., Boyd, D. D., Bent, P., Henderson, B. S., Pascioni, K. A., Sargent, D. C., Josephson, D. L., Marsan, M., He, H. B., et al., "Urban air mobility noise: Current practice, gaps, and recommendations," Tech. rep., 2020.
- [3] Meloni, S., de Paola, E., Grande, E., Ragni, D., Stoica, L., Di Marco, A., and Camussi, R., "A wavelet-based separation method for tonal and broadband components of low Reynolds-number propeller noise," *Measurement Science and Technology*, Vol. 34, No. 4, 2023, p. 044007.
- [4] Zhou, W., Ning, Z., Li, H., and Hu, H., "An experimental investigation on rotor-to-rotor interactions of small UAV propellers," *35th AIAA applied aerodynamics conference*, 2017, p. 3744.
- [5] Thai, A. D., De Paola, E., Di Marco, A., Stoica, L. G., Camussi, R., Tron, R., and Grace, S. M., "Experimental and computational aeroacoustic investigation of small rotor interactions in hover," *Applied Sciences*, Vol. 11, No. 21, 2021, p. 10016.

- [6] Alvarez, E. J., and Ning, A., “Modeling multirotor aerodynamic interactions through the vortex particle method,” *AIAA Aviation 2019 Forum*, 2019, p. 2827.
- [7] Grande, E., Romani, G., Ragni, D., Avallone, F., and Casalino, D., “Aeroacoustic investigation of a propeller operating at low Reynolds numbers,” *AIAA Journal*, Vol. 60, No. 2, 2022, pp. 860–871.
- [8] Zhou, T., Jiang, H., and Sun, X., “Noise source imaging measurements for small-scale multi-propeller systems,” *Applied Acoustics*, Vol. 194, 2022, p. 108801.
- [9] Lee, H., and Lee, D.-J., “Rotor interactional effects on aerodynamic and noise characteristics of a small multirotor unmanned aerial vehicle,” *Physics of Fluids*, Vol. 32, No. 4, 2020.
- [10] de Vries, R., van Arnhem, N., Sinnige, T., Vos, R., and Veldhuis, L. L., “Aerodynamic interaction between propellers of a distributed-propulsion system in forward flight,” *Aerospace Science and Technology*, Vol. 118, 2021, p. 107009.
- [11] Zarri, A., Koutsoukos, A., and Avallone, F., “Aerodynamic and Acoustic Interaction Effects of Adjacent Propellers in Forward Flight,” *AIAA AVIATION 2023 Forum*, 2023, p. 4489.
- [12] Zhou, T., and Fattah, R., “Tonal noise characteristics of two small-scale propellers,” *AIAA paper*, Vol. 4054, 2017, p. 2017.
- [13] Schiller, N. H., Pascioni, K. A., and Zawodny, N. S., “Tonal noise control using rotor phase synchronization,” *Vertical Flight Society Annual Forum and Technology Display (VFS Forum 75)*, 2019.
- [14] Pascioni, K., and Rizzi, S. A., “Tonal noise prediction of a distributed propulsion unmanned aerial vehicle,” *2018 AIAA/CEAS Aeroacoustics Conference*, 2018, p. 2951.
- [15] Bu, H., Wu, H., Bertin, C., Fang, Y., and Zhong, S., “Aerodynamic and acoustic measurements of dual small-scale propellers,” *Journal of Sound and Vibration*, Vol. 511, 2021, p. 116330.
- [16] Bu, H., Ma, Z., and Zhong, S., “An experimental investigation of noise characteristics of overlapping propellers,” *The Journal of the Acoustical Society of America*, Vol. 152, No. 1, 2022, pp. 591–600.